AGU PUBLICATIONS

Geophysical Research Letters

RESEARCH LETTER
10.1002/2014GL062032

Key Points:
- Fe-rich basalts are viable carriers of Mars magnetic anomalies
- Fe-rich basalts containing multidomain Fe-Ti oxides acquire intense NRM and ARM
- NRM preservation requires pressure effects or exsolution to increase coercivity

Supporting Information:
- Readme
- Figure S1
- Table S1
- Table S2
- Table S3

Correspondence to:
S. Brachfeld,
brachfelds@mail.montclair.edu

Citation:
Brachfeld, S., D. Cuomo, L. Tatsumi-Petrochilos, J. A. Bowles, D. Shah, and J. Hammer (2014), Contribution of multidomain titanomagnetite to the intensity and stability of Mars crustal magnetic anomalies, *Geophys. Res. Lett.*, *41*, 7997–8005, doi:10.1002/2014GL062032.

Received 27 SEP 2014
Accepted 15 OCT 2014
Accepted article online 18 OCT 2014
Published online 26 NOV 2014

Contribution of multidomain titanomagnetite to the intensity and stability of Mars crustal magnetic anomalies

Stefanie Brachfeld[1], David Cuomo[1], Lisa Tatsumi-Petrochilos[2], Julie A. Bowles[3], Deepa Shah[1], and Julia Hammer[2]

[1]Department of Earth and Environmental Studies, Montclair State University, Montclair, New Jersey, USA, [2]Department of Geology and Geophysics, University of Hawai'i, Honolulu, Hawai'i, USA, [3]Department of Geosciences, University of Wisconsin-Milwaukee, Milwaukee, Wisconsin, USA

Abstract Two basalts with compositions relevant to the crusts of Mars and Earth were synthesized at igneous temperatures and held at 650°C for 21 to 257 days under quartz-fayalite-magnetite fO_2 buffer conditions. The run products are germane to slowly cooled igneous intrusions, which might be a significant volumetric fraction of the Martian crust and carriers of magnetic anomalies in the Southern Highlands. Both basalts acquired intense thermoremanent magnetizations and intense but easily demagnetized anhysteretic remanent magnetizations carried by homogeneous multidomain titanomagnetite. Hypothetical intrusions on Mars composed of these materials would be capable of acquiring intense remanences sufficient to generate the observed anomalies. However, the remanence would be easily demagnetized by impact events after the cessation of the Mars geodynamo. Coercivity enhancement by pressure or formation of single domain regions via exsolution within the multidomain grains is necessary for long-term retention of a remanence carried exclusively by multidomain titanomagnetite grains.

1. Introduction

The high intensity of the Martian magnetic anomalies mapped by the Mars Global Surveyor (MGS) mission has led to considerable interest in the magnetization of the Martian crust, including the remanence acquisition process, composition of the magnetic recording assemblage, and subsequent modification of the remanence by impacts, volcanism, and near surface processes [*Acuña et al.*, 1999, 2001; *Connerney et al.*, 1999; *Hood et al.*, 2003; *Mohit and Arkani-Hamed*, 2004; *Shahnas and Arkani-Hamed*, 2007]. The magnetic anomalies are more intense (up to 250 nT at ~400 km altitude as per *Lillis et al.* [2008]) than the largest terrestrial anomaly. The magnetic field on Mars likely exhibited a range of intensities comparable to the terrestrial magnetic field [*Antretter et al.*, 2003; *Weiss et al.*, 2008]. Therefore, a very efficient and robust carrier of remanent magnetization must be present in the Martian crust to acquire and retain intense anomalies after exposure to shock and thermal demagnetization processes associated with impact events.

A previous set of investigations into the magnetic recording assemblage on Mars used synthetic basalts as analogs of Mars' crustal material [*Hammer*, 2006; *Brachfeld and Hammer*, 2006; *Bowles et al.*, 2009]. These studies explored the effects of chemical composition, oxygen fugacity (fO_2), and cooling history on the bulk mineralogy, mineral textures, magnetic mineralogy, magnetic domain state, and remanence carrying properties of the run products. These studies found that samples synthesized under moderately oxidizing conditions, within one $\log_{10}$ unit of the quartz-fayalite-magnetite (QFM) reference buffer, acquired intense thermoremanent magnetizations (TRM) even in relatively weak applied fields. Moderately oxidizing conditions, such as those that exist in the terrestrial crust, must have existed on early Mars in order to produce basalts capable of generating the observed crustal anomalies. Further, synthesis at QFM conditions coupled with fast cooling rates (3–231°C/h, relevant to rapidly cooled extrusive rocks) optimized TRM acquisition, with samples possessing stable-single-domain grains and TRM intensities exceeding 25 A/m [*Brachfeld and Hammer*, 2006; *Bowles et al.*, 2009].

Estimates of the thickness of the magnetized layer on Mars range from 35 to 100 km [*Nimmo and Gilmore*, 2001; *Arkani-Hamed*, 2003, 2005; *Voorhies*, 2008]. Some portion of the magnetized layer likely consists of subsurface intrusions as suggested by: (1) cumulate textures observed in SNC meteorites; (2) Mars Orbiter

Camera images of the Valles Marineris that resemble layered cumulate formations on Earth; (3) the absence of magnetic anomalies in the Tharsis region, suggesting subsurface thermal demagnetization of the crust by intrusions after the cessation of the geodynamo; and (4) geometric models of the sources of the Mars crustal field that are consistent with sub-surface dike swarms [*McSween*, 1994; *Nimmo*, 2000; *Williams et al*., 2003; *Johnson and Phillips*, 2005; *Hood et al*., 2007; *Ogawa and Manga*, 2007; *Lillis et al*., 2009]. The TRM recording and retention ability of Martian intrusive rocks may be quite different from rapidly cooled extrusive flows. Therefore, analogs of slow-cooled crustal materials are necessary to develop a more complete picture of Mars' crustal anomalies and their long-term stability.

We previously reported the results of experiments designed to investigate exsolution mechanisms and time-dependent changes in iron oxide mineral textures and domain states [*Petrochilos*, 2010; *Bowles et al*., 2012]. Here we describe a subset of those experimental runs in which we observed neither petrographic nor magnetic evidence supporting oxide exsolution. However, the crystallization and anneal conditions are germane to slowly cooled igneous intrusions, and the results provide an important contrast to the previous sets of fast-cooled experiments our group performed on similar basalt compositions [*Brachfeld and Hammer*, 2006; *Bowles et al*., 2009].

2. Materials and Methods

The basalt synthesis process is described in *Petrochilos* [2010]. Bulk chemical compositions and normative mineralogy of two synthetic basalts and the materials on which they are patterned are given in Table S1 and described in *Bowles et al*. [2009]. "M-type" basalt is patterned after the composition of Mars basaltic meteorite Chassigny A [*Johnson et al*., 1991]. The T-type composition is similar to Medicine Lake Highland basalt 82-66 [*Sisson and Grove*, 1993], a high alumina basalt that is consistent with thermal emission spectrometer constraints on the composition of Mars' surface [*Hamilton et al*., 2001].

The M-type composition is poor in Al and rich in Fe (Fe/Al = 1.4), reflecting the composition of basaltic liquid in equilibrium with Martian meteorite phase assemblages. The T-type composition is rich in Al and poor in Fe (Fe/Al = 0.3) (Table S1). Other differences include silica content (the T-type composition is silica undersaturated, whereas the M-type composition is quartz-normative), normative Fe-Ti oxide speciation (T-type contains double the normative ilmenite and ~40% of the normative magnetite of M-type), and calcium content (giving rise to differences in normative pyroxene and feldspar contents) (Table S1). Although the terrestrial T-type composition is unlikely to represent a majority of the Martian crust [*McSween et al*., 2009], it is included to provide a counterpart to the Fe-rich, Al-poor M-type basalts associated primarily with meteorite samples and allow evaluation of the major-element control on magnetic and mineralogical variations in the Mars crust.

Batches of each composition were cooled from >1200°C to 1070°C at 4°C/h, held at 1070°C for 100 h in a Fe-soaked 5 mL platinum crucible, and then quenched to form the starting materials for a lower-temperature "anneal" step. During the anneal step, samples were held in evacuated silica glass tubes at 650°C for periods ranging from 21 to 257 days, and then quenched. A solid assemblage of quartz + fayalite + magnetite (QFM) was included in each tube as a monitor of fO_2 buffer conditions. The two-stage experiments effectively isolate the high-temperature and low-temperature synthesis steps, as a practical simplification of the complex thermal history typifying subsurface magma cooling. The two-stage strategy also represents the solution to furnace temperature and fO_2 control limitations over a wide range in temperature. Six pairs of experiments, representing anneal durations of 21, 32, 48, 111, 158, and 257 days were characterized petrographically and magnetically.

Splits of the run products were made for electron microscopy and rock magnetic analyses. Electron microprobe analyses were conducted on a JEOL JXA-8500F Field Emission Hyperprobe at the University of Hawai'i at Mānoa. Low-field mass-normalized magnetic susceptibility (χ_{LF}) was measured on an AGICO KLY-4 Kappabridge. The natural remanent magnetization (NRM) and anhysteretic remanent magnetization (ARM) were measured on a 2G-Enterprises Model 755 magnetometer at Lehigh University and on an AGICO JR6 spinner magnetometer at Montclair State University. ARM was imparted in a 100 mT peak alternating field and a 98 μT DC bias field. Stepwise alternating field (AF) demagnetization data were used to calculate the median destructive field (MDF) of the ARM.

Magnetic hysteresis measurements were made on a Princeton Measurements Corp. micro-Vibrating Sample Magnetometer (VSM) model 3900-04 at Montclair State University, NJ. Hysteresis loops were measured in a peak field of 1 T and field increments of 5 mT and corrected for the paramagnetic contribution to the induced magnetization. The hysteresis parameters saturation magnetization (M_S), saturation remanence (M_R), and

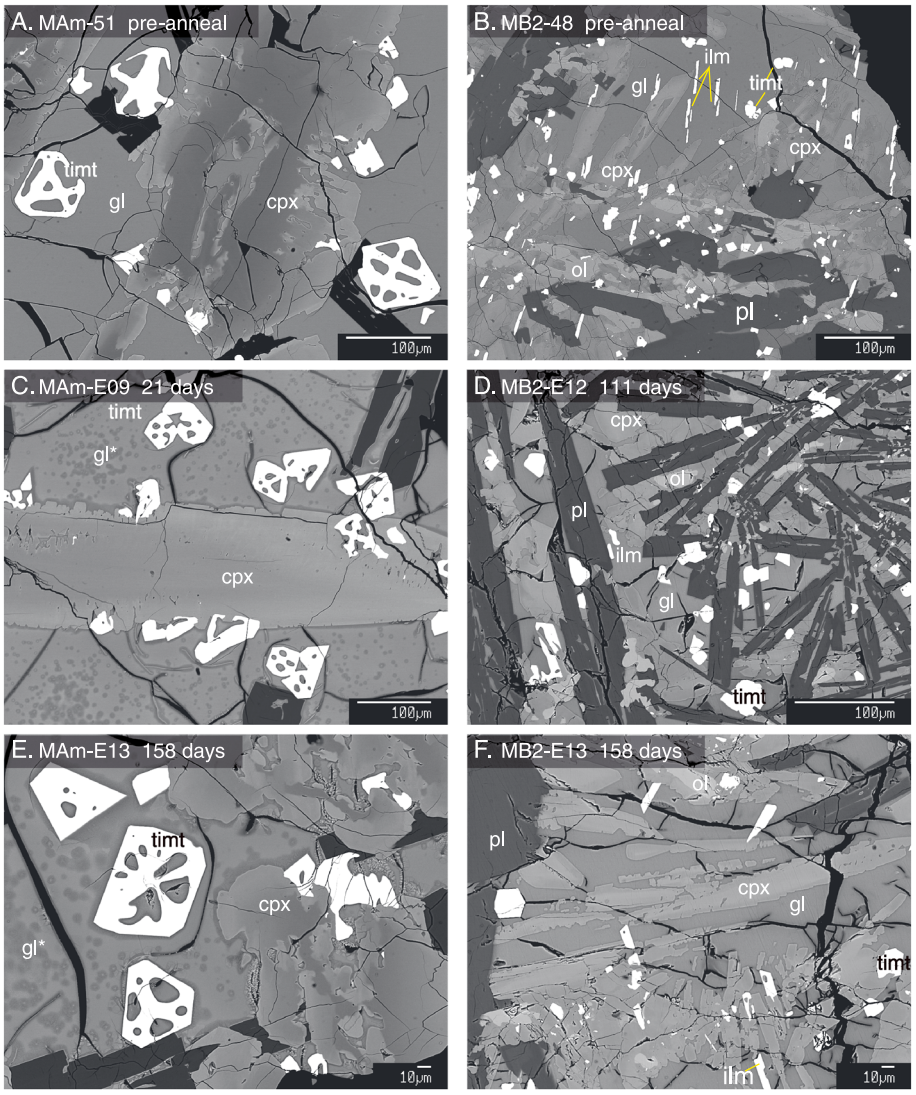

Figure 1. Backscatter electron (BSE) images of M-type (left column) and T-type (right column) pre-anneal starting materials, and run products after annealing at 650°C. (a) M-type pre-anneal starting material. (b) T-type pre-anneal starting material. (c) M-type sample annealed for 21 days. (d) T-type samples annealed for 111 days. (e, f) M-type and T-type samples annealed for 158 days. Major phases include titanomagnetite (equant white grains labeled timt), ilmenite (elongated white grains labeled ilm), clinopyroxene (light gray grains), plagioclase (darkest gray-black rectangular grains), glass (intermediate grey regions labeled gl), and glass undergoing devitrification (denoted gl*).

coercivity (H_C) were determined from the paramagnetic-corrected data. The coercivity of remanence (H_{CR}) was determined through the DC-demagnetization of a saturation isothermal remanent magnetization imparted in a 1 T field. Curie temperatures (T_C) were measured on the VSM in a flowing helium gas atmosphere. We monitored the induced magnetization in a 50 mT applied field as a function of temperature from 25 to 700°C. All rock magnetic parameters measured are reported in Table S2. In addition, low temperature magnetic measurements are shown in Figure S1.

3. Results

3.1. Mineral Assemblages and Textures

The phase assemblage in the M-type starting material (sample ID MAm-51) in order of decreasing abundance is clinopyroxene, glass, plagioclase, and Mg- and Al-bearing titanomagnetite (Figure 1). The glass in this sample results from quenching the starting material at 1070°C while the melt was still above the solidus

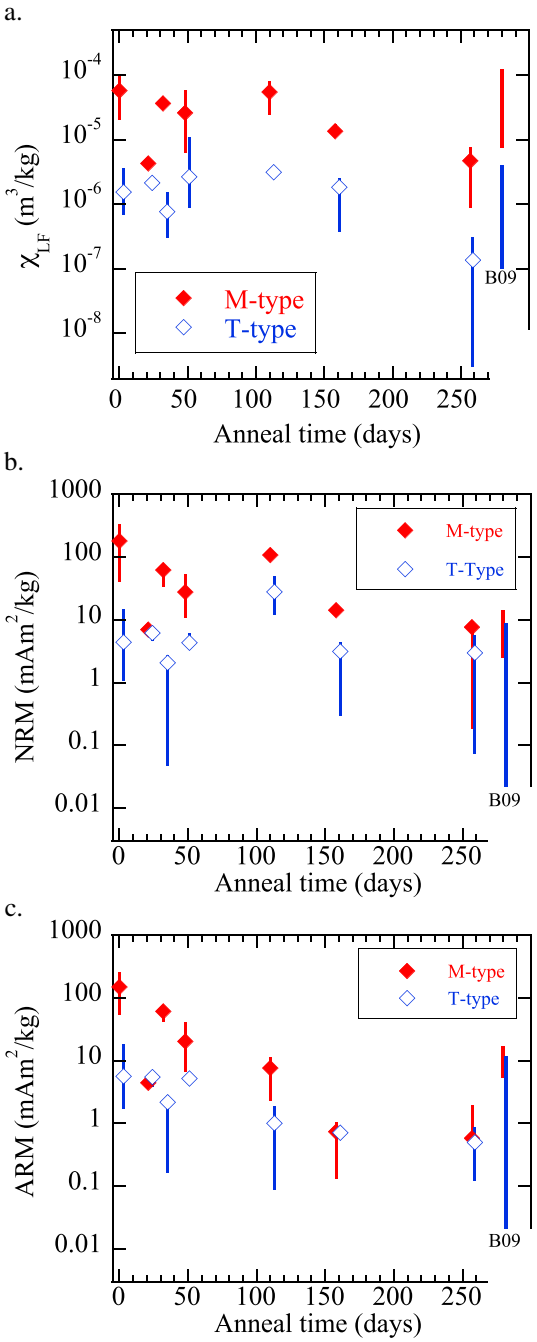

Figure 2. (a) Low field magnetic susceptibility (x_{LF}), (b) natural remanent magnetization (NRM), and (c) anhysteretic remanent magnetization (ARM) as a function of anneal time. Vertical lines show the range of values observed in individual sample chips. Solid and open symbols are the calculated weighted average (by mass) for M-type and T-type samples, respectively. Vertical lines labeled B09 show the range of values for rapidly cooled (6–231°C/h) basalts described in *Bowles et al.* [2009].

(est. ~950°C according to the MELTS model; *Ghiorso and Sack* [1995]). Clinopyroxene crystals are subhedral, elongated, and blocky with a slight but complex zoning (Figure 1a). Plagioclase occurs as euhedral tabular crystals. Titanomagnetite crystals are euhedral, equant, and ~30–80 μm in diameter (Figure 1a), well within the multidomain size region, and much larger than those produced in the rapidly cooled samples of the same composition [*Bowles et al.*, 2009]. We also observed rounded and equant titanomagnetite grains 5–10 μm in diameter (in the pseudo-single-domain field for titanomagnetite) that occur in clusters. In contrast to their rapidly cooled counterparts, there are no oxides smaller than approximately 5 μm visible in the electron microscopy images.

The annealed samples (MAm-E09-E16) using this starting material have the same phase assemblage as the starting material. Backscatter electron images reveal no discernable bulk mineralogical differences with anneal time (Figure 1). However, we observe that the concentrations of MgO and TiO_2 in the titanomagnetite decrease 2–4% with increasing anneal time, and we observe an increasing devitrification in the glass with increasing anneal time [*Petrochilos*, 2010] (Table S3).

The phase assemblage in the T-type starting material (MB2-48) in order of decreasing abundance is plagioclase, clinopyroxene, glass (solidus estimated at 895°C; *Ghiorso and Sack* [1995]), Mg-, Al-, and Cr-bearing titanomagnetite, olivine, and ilmenite. Plagioclase occurs as faceted, highly elongated hopper crystals (Figure 1b). Clinopyroxene crystals in this sample are faceted subhedral with a slight but complex zoning evident as concentric Z-contrast in BSE imaging (Figure 1). Olivine crystals are anhedral. Titanomagnetite crystals are euhedral, equant, and generally 5–10 μm in diameter. The T-type titanomagnetites have more Ti, Mg, and Cr than their M-type counterparts. Ilmenite crystals are euhedral and elongated, approximately 5 μm wide and 30 μm in length (Figure 1b).

The time-dependent annealed samples (MB2 E09–E16) using the T-type starting material have the same phase assemblage and texture as the starting material, and also show increasing devitrification in the glass with increasing anneal time (Figure 1). The amount of MgO and TiO_2 in titanomagnetite and ilmenite decreases ~2–4% with anneal time [*Petrochilos*, 2010] (Table S3). The run annealed for 48 days (MB2-E11) contains sparse grains with a Cr-rich core surrounded by a titanomagnetite rim, as well as Cr-rich

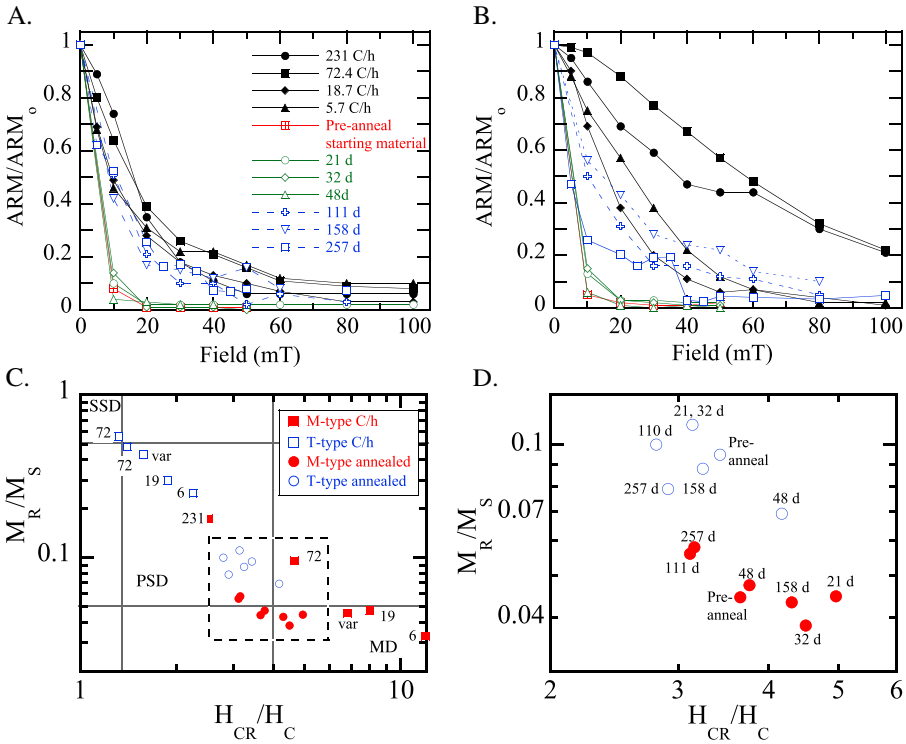

Figure 3. Step-wise alternating field demagnetization of ARM in (a) M-type and (b) T-type basalts. Solid symbols denote rapidly cooled basalts from *Bowles et al.* [2009]. Open symbols denote variable duration anneal period (this study). Samples annealed for 111, 158, and 257 days have alternating field (AF) demagnetization spectra that approach the slowest (5.7°C/h) of the rapidly cooled samples. (c) Hysteresis parameters for annealed samples compared with their rapidly cooled counterparts of the same chemical compositional and fO_2 synthesis conditions. Data are displayed as saturation remanence normalized by saturation magnetization (M_R/M_S) vs. coercivity of remanence normalized by coercivity (H_{CR}/H_C). Numbers next to symbols denote the cooling rate (C/h) of rapidly cooled samples [*Bowles et al.*, 2009]. (d) Close-up of boxed region in Figure 3c. Numbers next to symbols denote anneal period in days.

grains without zoning. This is the only sample in which such grains are observed, which we interpret as arising from heterogeneity in the starting material or the statistical improbability of encountering sparse grains in a random section plane.

3.2. Magnetic Properties

Three to five chips with masses of a few milligrams to several tens of milligrams were measured from each run product. The chips are heterogeneous, likely due to gravitational settling of crystals within the 5 mL platinum crucibles, resulting in differing amounts of Fe-oxides within each chip. Maximum and minimum values for each parameter are shown in Figure 2. A weighted average value (by mass) was calculated for all chips from each run and reported in Table S2. Susceptibility values range from 7 to 97×10^{-6} m^3/kg for M-type samples and 0.3 to 11×10^{-6} m^3/kg for T-type samples (Table S2 and Figure 2). Both M-type and T-type samples possess a strong NRM (Table TS01 and Figure 2). The NRM is inferred to be a TRM acquired during quenching and air cooling after the 650°C anneal in the ambient laboratory field (approximately 35 μT). NRM values range from 7 to 107.6 mAm^2/kg for M-type samples, and up to 315 mAm^2/kg in individual chips of the pre-anneal M-type starting material. NRM values in T-type samples range from 2.1 to 28.1 mAm^2/kg. ARM values range from 0.6 to 60.6 mAm^2/kg in M-type samples and up to 149 mAm^2/kg in the pre-anneal starting material. MAm-E12 and MB2-E12 both have high NRM intensities relative to the other annealed samples (Table S2), as well as high values of susceptibility and saturation magnetization. ARM values range from 0.5 to 5.5 mAm^2/kg in T-type samples, and up to 14 mAm^2/kg in individual chips of the pre-anneal starting material (Figure 2 and Table S2).

Following NRM measurements, the samples were demagnetized in a 100 mT peak alternating field in three perpendicular directions prior to imparting ARM. After imparting ARM, the samples were stepwise

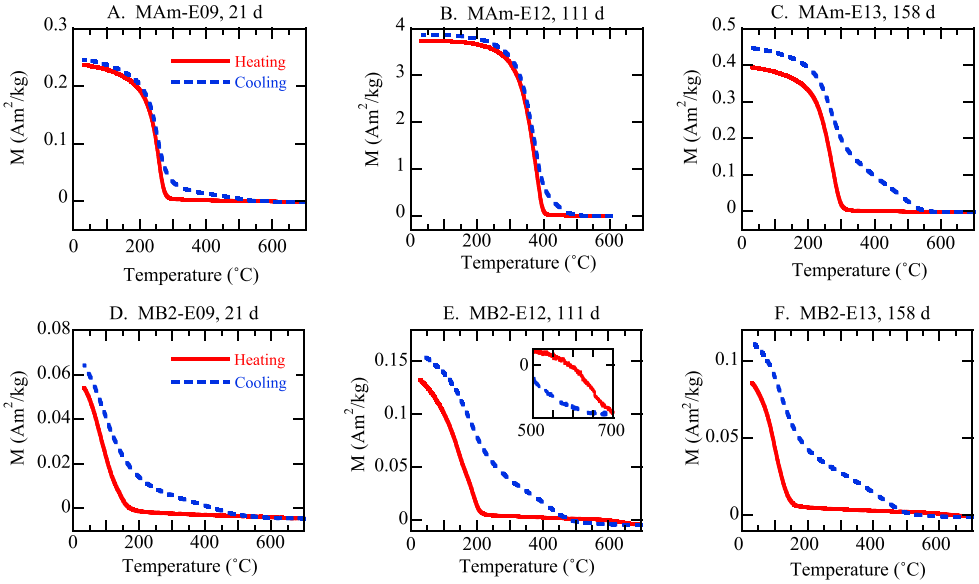

Figure 4. Induced magnetization in a 50 mT applied field vs. temperature for (a–c) M-type and (d–f) T-type samples.

AF demagnetized in peak fields of 0 to 100 mT. M-type samples (Figure 3a) were easily AF demagnetized. In the M-type samples <10% of the remanence remained after the first demagnetization step at 10 mT. Samples annealed for 111 to 257 days had slightly harder AF demagnetization spectra, with 40–50% of remanence remaining after the 10 mT demagnetization step. Similarly, T-type samples annealed for 111 to 257 days had approximately 34–55% of the remanence remaining after the 10 mT demagnetization step (Figure 3b). Hysteresis parameters for M-type samples plot within the multidomain region of a Day Plot [*Day et al.*, 1977]. T-type samples plot in the lower right corner of the pseudo-single domain (PSD) region (Figures 3c and 3d).

M-type samples have Curie temperatures (T_c) that range from 285 to 410°C (Figures 4a–4c). The heating and cooling curves are generally reversible for anneal times <111 days. Samples annealed for ≥111 days were more susceptible to alteration during heating. T-type samples have Curie temperatures between 130 and 215°C [*Bowles et al.*, 2009 and Figures 4d–4f]. T-type samples additionally display a subtle, continuous decrease in M_S between 500 and 700°C (Figure 4e inset), suggestive of hematite, which may be present as nanno-scale intergrowths with ilmenite. Heating and cooling curves for the T-type samples are not reversible, and the cooling curves are stronger than the heating curves.

4. Discussion

The NRM and ARM values recorded by the slow-cooled samples are comparable to, and even exceed, the TRM induced in rapidly cooled synthetic basalts of the same chemical composition [*Bowles et al.*, 2009]. We observed no systematic relationship between NRM and ARM intensity and anneal period. However, the annealed samples generally have lower intensities of NRM and ARM than their starting materials. Annealing removes defects and dislocations from materials, which serve as pinning points for domain walls in multidomain iron oxides and contribute to remanence acquisition and retention. The annealing process may have reduced the efficiency of remanence acquisition and retention in these multidomain oxides, as suggested by the soft ARM AF demagnetization spectra of the annealed samples (Figure 3).

Both M-type and T-type samples with anneal periods longer than 111 days have slightly harder AF demagnetization spectra (Figure 3) and elevated NRM/ARM ratios (Table S3). Both M-type and T-type samples contain devitrification textures within the glass, with the amount of glass devitrification increasing with anneal time (Figure 1). We speculate that stable-single-domain (SSD) iron oxides below the resolution of the electron microprobe are forming during devitrification, leading to more PSD-like hysteresis loops, enhanced TRM acquisition, and harder AF demagnetization spectra in our annealed samples, which has also been observed in natural and synthetic basaltic glasses [*Burgess et al.*, 2010;

Bowles et al., 2011]. The high amount of glass in these samples is a function of quenching the pre-anneal starting materials. We do not expect these conditions to occur in nature, where slowly cooled intrusions should be holocrystalline. However, the growth of SSD oxides during devitrification is relevant to basaltic glasses at the Martian surface. The effect of this phenomenon on the amplitude of crustal anomalies depends on the timing of both dynamo cessation and oxide growth. Basalts would carry a TRM if devitrification and growth of SSD oxides occurred while the basalt temperature was above the blocking temperature (T_B) of the magnetic mineral assemblage, a chemical remanent magnetization (CRM) if the devitrification occurred below T_B but in the presence of a dynamo field, or a combination of both depending on the relative timing of cooling and oxide growth.

The Curie temperatures of the annealed M-type samples are comparable to those observed in their rapidly cooled counterparts of the same composition [*Bowles et al.*, 2009]. The T-type samples reported here have lower Curie temperatures than their rapidly cooled counterparts. Curie temperatures in both M-type and T-type annealed samples increase slightly as a function of anneal duration. This is consistent with EMPA data that show oxides becoming very slightly more iron-rich at longer anneal times. For our purposes, T_C is used to predict the depth to the Curie isotherm rather than as a diagnostic material property. For linear geothermal gradients of 5–20°C/km, the depth to the Curie isotherm is approximately 15 to 80 km for an M-type layer, and 7 to 45 km for a T-type layer.

Using simple geometric models of a uniformly magnetized prism [*Nimmo*, 2000; *Brachfeld and Hammer*, 2006] the high-intensity NRM values recorded by the M-type annealed samples (20–312 A/m using a density of 2900 kg/m^3 for conversion to volume-normalized units) are more than sufficient to generate the observed anomalies at satellite altitude within the layer thickness constrained by the M-type Curie temperatures. The majority of T-type annealed samples have volume-normalized remanences of 6–18 A/m, which is insufficient to generate the observed anomalies at satellite altitude in a layer thickness constrained by T-type Curie temperatures. The exception is sample MB2-E12, which has an NRM intensity of 81.4 A/m. MB2-E12 and MAm-E12 (anneal time 111 d) have NRM/ARM ratios of 28 and 14, respectively, much higher than the samples with shorter anneal durations. These samples likely contain the greatest abundance of single domain grains formed during devitrification, which reinforces the importance of domain state and oxide concentration for acquiring and retaining crustal anomalies.

Although the M-type annealed samples carry an intense NRM, the soft coercivity spectra of these samples make it unlikely that a TRM or CRM carried by this material would be retained over geologic time. Iron oxides and iron sulfides experience shock-demagnetization beginning at pressures of less than 1 to 2 GPa, with continued loss of remanence with increasing pressure [e.g., *Hargraves and Perkins*, 1969; *Nagata*, 1971; *Cisowski and Fuller*, 1978; *Rochette et al.*, 2003; *Louzada et al.*, 2007, 2011; *Bezaeva et al.*, 2007, 2010]. *Bezaeva et al.* [2010] observed that a pressure of 1.24 GPa was sufficient to remove 84% of an induced isothermal remanent magnetization, with low coercivity samples more easily demagnetized than high-coercivity samples. The lack of crustal anomalies within and around the Hellas, Isidis, Utopia, and Argyre impact basins on Mars suggests that the original NRM carried by the Mars crust has been extensively modified by impact events [*Acuña et al.*, 1999; *Hood et al.*, 2003]. The cumulative effect of impacts on Mars may have demagnetized the upper 5–10 km of the crust after the dynamo field switched off [*Arkani-Hamed*, 2003; *Louzada et al.*, 2007, 2011; *Lillis et al.*, 2010], reducing the thickness of the magnetized layer.

An M-type intrusion containing exclusively multidomain grains and residing within 10 km of the planet's surface would be largely demagnetized, given its soft coercivity spectra. Intrusions that are deeper than the penetration depth of the 1–2 GPa shock pressure contours but above the Curie isotherm may still contribute to the Mars crustal anomalies via several mechanisms. *Gilder and Le Goff* [2008] demonstrated that saturation isothermal remanent magnetization (SIRM) and coercivity of remanence (as measured via H_{CR} and the median destructive field) increase in multidomain Ti-rich titanomagnetite ($x > 0.2$) as a function of pressure. They further observed that the Curie temperature is also elevated at high pressure [*Samara and Giardini*, 1969; *Schult*, 1970], and the combination of these enhancements may preserve an NRM carried by multidomain titanomagnetite in a planet's crust. In addition, if the multidomain oxides undergo exsolution during natural timescales for cooling, then the resulting increase in coercivity would make the basalts more resistant to shock demagnetization, and they may still contribute substantially to the crustal anomalies [*Robinson et al.*, 2002; *McEnroe et al.*, 2004].

5. Conclusions

M-type and T-type basalts studied here are dominated by multidomain titanomagnetite. The basalts display χ_{LF}, NRM, and ARM intensities comparable to or exceeding those of their rapidly cooled counterparts. The annealed samples have lower NRM and ARM intensities than their pre-anneal starting materials, which may result from the removal of defects and dislocations during annealing. The M-type composition is capable of generating intense magnetic anomalies at satellite altitude; the T-type composition in general is not, although one T-type sample with elevated χ_{LF} and M_S also has a very strong NRM. However, the ARM in the annealed samples is easily AF demagnetized, though slightly harder in samples annealed for 111 to 257 days. This hardening of the coercivity spectra is attributed to sub-micron iron oxides forming in glass during devitrification.

Our results have implications for the long-term stability of crustal anomalies carried by multidomain titanomagnetite assemblages. The low coercivity of both compositions suggests that these materials, if located near the Martian surface, would be shock demagnetized during impact events. Retention of the remanent magnetization carried by multidomain titanomagnetite is only possible at greater depths where high pressure enhances coercivity in Ti-rich titanomagnetites. Alternately, exsolution of multidomain grains during cooling over natural timescales could also enhance coercivity and resistance to shock demagnetization.

Acknowledgments

We thank Andrew Dombard for editorial assistance and two anonymous reviewers for helpful comments that improved this manuscript. We thank Ken Kodama of Lehigh University for the use his facilities for NRM and ARM measurements. Low temperature experiments were performed at the Institute for Rock Magnetism, University of Minnesota, during a visiting fellowship to S.B. All magnetic data presented in this paper are available from the Magnetics Information Consortium (MagIC) database (earthref.org/MAGIC/). This work was supported by NASA grants NAG5-12486, MFR04-0000-0021, and NNX11AM29G, and NSF-EAR/IF grant 0948262.

Andrew Dombard thanks one anonymous reviewer for his assistance in evaluating this paper.

References

Acuña, M. H., et al. (1999), Global Distribution of Crustal Magnetization Discovered by the Mars Global Surveyor MAG/ER Experiment, *Science*, *284*, 790–793, doi:10.1126/science.284.5415.790.

Acuña, M. H., et al. (2001), Magnetic field of Mars: Summary of results from the aerobraking and mapping orbits, *J. Geophys. Res.*, *106*, 23,403–23,417, doi:10.1029/2000JE001404.

Antretter, M., M. Fuller, E. Scott, M. Jackson, B. Moskowitz, and P. Sølheid (2003), Paleomagnetic record of Martian meteorite ALH84001, *J. Geophys. Res.*, *108*(E6), 5049, doi:10.1029/2002JE001979.

Arkani-Hamed, J. (2003), Thermoremanent magnetization of the Martian lithosphere, *J. Geophys. Res.*, *108*(E10), 5114, doi:10.1029/2003JE002049.

Arkani-Hamed, J. (2005), Magnetic crust of Mars, *J. Geophys. Res.*, *110*, E08005, doi:10.1029/2004JE002397.

Bezaeva, N. S., P. Rochette, J. Gattacceca, R. A. Sadykov, and V. I. Trukhin (2007), Pressure demagnetization of the Martian crust: Ground truth from SNC meteorites, *Geophys. Res. Lett.*, *34*, L23202, doi:10.1029/2007GL031501.

Bezaeva, N. S., J. Gattaccecca, P. Rochette, R. A. Sadykov, and V. I. Trukhin (2010), Demagnetization of terrestrial and extraterrestrial rocks under hydrostatic pressure up to 1.2 GPa, *Phys. Earth Planet. Int.*, *179*, 7–20, doi:10.1016/j.pepi.2010.01.004.

Bowles, J., J. Hammer, and S. Brachfeld (2009), Magnetic and petrologic characterization of synthetic Martian basalts and implications for the surface magnetization of Mars, *J. Geophys. Res.*, *114*, E10003, doi:10.1029/2009JE003378.

Bowles, J. A., J. S. Gee, K. Burgess, and R. F. Cooper (2011), Timing of magnetite formation in basaltic glass: Insights from synthetic analogs and relevance for geomagnetic paleointensity analyses, *Geochem. Geophys. Geosyst.*, *12*, Q02001, doi:10.1029/2010GC003404.

Bowles, J. A., L. Tatsumi-Petrochilos, J. E. Hammer, and S. A. Brachfeld (2012), Multi-component cubic oxide exsolution in synthetic basalts: Temperature dependence and implications for magnetic properties, *J. Geophys. Res.*, *117*, B03202, doi:10.1029/2011JB008867.

Brachfeld, S. A., and J. E. Hammer (2006), Rock-magnetic and remanence properties of synthetic Fe-rich basalts: Implications for Mars crustal anomalies, *Earth Planet. Sci. Lett.*, *248*, 599–617, doi:10.1016/j.epsl.2006.04.015.

Burgess, K., R. F. Cooper, J. A. Bowles, J. S. Gee, and D. J. Cherniak (2010), Effects of open and closed system oxidation on texture and magnetic response of remelted basaltic glass, *Geochem. Geophys. Geosyst.*, *11*, Q10007, doi:10.1029/2010GC003248.

Cisowski, S. M., and M. Fuller (1978), The effect of shock on the magnetism of terrestrial rocks, *J. Geophys. Res.*, *83*(B7), 3441–3458, doi:10.1029/JB083iB07p03441.

Connerney, J. E. P., M. H. Acuña, P. J. Wasilewski, N. F. Ness, H. Rème, C. Mazelle, D. Vignes, R. P. Lin, D. L. Mitchell, and P. A. Cloutier (1999), Magnetic lineations in the ancient crust of Mars, *Science*, *284*, 749–798, doi:10.1126/science.284.5415.794.

Day, R., M. D. Fuller, and M. V. A. Schmidt (1977), Hysteresis properties of titanomagnetites: Grain size and composition dependence, *Phys. Earth Planet. Int.*, *13*, 260–266, doi:10.1016/0031-9201(77)90108-X.

Ghiorso, M. S., and R. O. Sack (1995), Chemical mass transfer in magmatic processes IV. A revised and internally consistent thermodynamic model for the interpolation and extrapolation of liquid-solid equilibria in magmatic systems at elevated temperatures and pressures, *Contrib. Mineral. Petrol.*, *119*, 197–212, doi:10.1007/BF00307281.

Gilder, S. A., and M. Le Goff (2008), Systematic pressure enhancement of titanomagnetite magnetization, *Geophys. Res. Lett.*, *35*, L10302, doi:10.1029/2008GL033325.

Hamilton, V. E., M. B. Wyatt, H. Y. McSween Jr., and P. R. Christensen (2001), Analysis of terrestrial and Martian volcanic compositions using thermal emission spectroscopy: 2. Application to Martian surface spectra from the Mars Global Surveyor Thermal Emission Spectrometer, *J. Geophys. Res.*, *106*, 14,733–14,746, doi:10.1029/2000JE001353.

Hammer, J. E. (2006), Influence of fO_2 and cooling rate on the kinetics and energetics of Fe-rich basalt crystallization, *Earth Planet. Sci. Lett.*, *248*, 618–637, doi:10.1016/j.epsl.2006.04.022.

Hargraves, R. B., and W. E. Perkins (1969), Investigations of the effect of shock on Natural remanent magnetization, *J. Geophys. Res.*, *74*, 2576–2589, doi:10.1029/JB074i010p02576.

Hood, L. L., N. C. Richmond, E. Pierazzo, and P. Rochette (2003), Distribution of crustal magnetic fields on Mars: Shock effects of basin-forming impacts, *Geophys. Res. Lett.*, *30*(6), 1281–1284, doi:10.1029/2002GL016657.

Hood, L. L., N. C. Richmond, K. P. Harrison, and R. J. Lillis (2007), East-west trending magnetic anomalies in the Southern Hemisphere of Mars: Modeling analysis and interpretation, *Icarus*, *191*, 113–131, doi:10.1016/j.icarus.2007.04.025.

Johnson, C. L., and R. J. Phillips (2005), Evolution of the Tharsis region of Mars: Insights from magnetic field observations, *Earth Planet. Sci. Lett.*, *230*, 241–254, doi:10.1016/j.epsl.2004.10.038.

Johnson, M. C., M. J. Rutherford, and P. C. Hess (1991), Chassigny petrogenesis melt compositions, intensive parameters, and water contents of Martian (?) magmas, *Geochim. Cosmochim. Acta*, *55*, 349–366.

Lillis, R. J., H. V. Frey, M. Manga, D. L. Mitchell, R. P. Lin, M. H. Acuña, and S. W. Bougher (2008), An improved crustal magnetic field map of Mars from electron reflectometry: Highland volcano magmatic history and the end of the martian dynamo, *Icarus*, *194*, 575–596, doi:10.1016/j.icarus.2007.09.032.

Lillis, R. J., J. Dufek, J. E. Bleacher, and M. Manga (2009), Demagnetization of crust by magmatic intrusion near the Arsia Mons volcano: Magnetic and thermal implications for the development of the Tharsis province, Mars, *J. Volcanol. Geotherm. Res.*, doi:10.1016/j.jvolgeores.2008.12.007.

Lillis, R. J., M. E. Purucker, J. S. Halekas, K. L. Louzada, S. T. Stewart-Mukhopadhyay, M. Manga, and H. V. Frey (2010), Study of impact demagnetization at Mars using Monte Carlo modeling and multiple altitude data, *J. Geophys. Res.*, *115*, E07007, doi:10.1029/2009JE003556.

Louzada, K. L., S. T. Stewart, and B. P. Weiss (2007), Effect of shock on the magnetic properties of pyrrhotite, the Martian crust, and meteorites, *Geophys. Res. Lett.*, *34*, L05204, doi:10.1029/2006GL027685.

Louzada, K. L., S. T. Stewart, B. P. Weiss, J. Gattacceca, R. J. Lillis, and J. S. Halekas (2011), Impact demagnetization of the Martian crust: Current knowledge and future directions, *Earth Planet. Sci. Lett.*, *305*, 257–269, doi:10.1016/j.epsl.2011.03.013.

McEnroe, S. A., J. R. Skilbrei, P. Robinson, F. Heidelbach, F. Langenhorst, and L. L. Brown (2004), Magnetic anomalies, layered intrusions and Mars, *Geophys. Res. Lett.*, *31*, L19601, doi:10.1029/2004GL020640.

McSween, H. Y. (1994), What we have learned about Mars from the SNC meteorites, *Meteoritics*, *29*, 757–779, doi:10.1111/j.1945-5100.1994.tb01092.x.

McSween, H. Y., G. J. Taylor, and M. B. Wyatt (2009), Elemental composition of the Martian Crust, *Science*, *324*, 736–739, doi:10.1126/science.1165871.

Mohit, P. S., and J. Arkani-Hamed (2004), Impact demagnetization of the Martian crust, *Icarus*, *168*, 305–317, doi:10.1016/j.icarus.2003.12.005.

Nagata, T. (1971), Introductory notes on shock remanent magnetization and shock demagnetization of igneous rocks, *Pure Appl. Geophys.*, *89*, 159–177, doi:10.1007/BF00875213.

Nimmo, F. (2000), Dike intrusion as a possible cause of linear martian magnetic anomalies, *Geology*, *28*, 391–394, doi:10.1130/0091-7613(2000)28<391:DIAAPC>2.0.CO;2.

Nimmo, F., and M. S. Gilmore (2001), Constraints on the depth of magnetized crust on Mars from impact craters, *J. Geophys. Res.*, *106*(E6), 12,315–12,323, doi:10.1029/2000JE001325.

Ogawa, Y., and M. Manga (2007), Thermal demagnetization of Martian upper crust by magma intrusion, *Geophys. Res. Lett.*, *34*, L16302, doi:10.1029/2007GL030565.

Petrochilos, L. T. (2010), Experimental and analytical studies of titanomagnetite in synthetic and natural samples, Masters thesis, 157 pp., Univ. of Hawai'i Manoa, Manoa, Hawaii.

Robinson, P., R. J. Harrison, S. A. McEnroe, and R. B. Hargraves (2002), Lamellar magnetism in the hematite-ilmenite series as an explanation for strong remanent magnetization, *Nature*, *418*, 517–520, doi:10.1038/nature00942.

Rochette, P., G. Fillion, R. Ballou, F. Brunet, B. Ouladdiaf, and L. Hood (2003), High pressure magnetic transition in pyrrhotite and impact demagnetization on Mars, *Geophys. Res. Lett.* *30*(13), 1683, doi:10.1029/2003GL017359.

Samara, G., and A. Giardini (1969), Effect of pressure on the Néel temperature of magnetite, *Phys. Rev.*, *186*, 577–580.

Schult, A. (1970), Effect of pressure on the Curie temperature of titanomagnetites [(1-x)•Fe_3O_4 – x•$TiFe_2O_4$], *Earth Planet. Sci. Lett.*, *10*, 81–86.

Shahnas, H., and J. Arkani-Hamed (2007), Viscous and impact demagnetization of Martian crust, *J. Geophys. Res.*, *112*, E02009, doi:10.1029/2005JE002424.

Sisson, T. W., and T. L. Grove (1993), Experimental investigations of the role of H_2O in calc-alkaline differentiation and subduction zone magmatism, *Contrib. Mineral. Petrol.*, *113*, 143–166.

Voorhies, C. V. (2008), Thickness of the magnetic crust of Mars, *J. Geophys. Res.*, *113*, E04004, doi:10.1029/2007JE002928.

Weiss, B. P., L. E. Fong, H. Vali, E. A. Lima, and F. J. Baudenbacher (2008), Paleointensity of the ancient Martian magnetic field, *Geophys. Res. Lett.*, *35*, L23207, doi:10.1029/2008GL035585.

Williams, J.-P., D. A. Paige, and C. E. Manning (2003), Layering in the wall rock of Valles Marineris: Intrusive and extrusive magmatism, *Geophys. Res. Lett.*, *30*(12), 1623, doi:10.1029/2003GL017662.